

Description and evaluation of a six-moment aerosol microphysical module for use in atmospheric chemical transport models

D. L. Wright and P. S. Kasibhatla

Nicholas School of the Environment, Duke University, Durham, North Carolina

R. McGraw and S. E. Schwartz

Atmospheric Sciences Division, Department of Applied Science, Brookhaven National Laboratory
Upton, New York

Abstract. We describe and evaluate a six-moment aerosol microphysical module, 6M, designed for implementation in atmospheric chemical transport models (CTMs). The module 6M is based upon the quadrature method of moments (QMOM) [McGraw, 1997] and the multiple isomomental distribution aerosol surrogate (MIDAS) method [Wright, 2000]. The module 6M evolves the lowest six radial moments of $\text{H}_2\text{SO}_4\text{-H}_2\text{O}$ aerosols for a comprehensive set of dynamical processes including the formation of new particles via binary $\text{H}_2\text{SO}_4\text{-H}_2\text{O}$ nucleation, condensational growth, coagulation, evolution due to cloud processing, size-resolved dry deposition, and water uptake and release with changing relative humidity. Performance of the moment-based aerosol evolution is examined and evaluated by comparison with results obtained using a high-resolution discrete model of the particle dynamics for a range of conditions representative of the boundary layer and lower troposphere. Overall, the performance of 6M is good relative to uncertainties associated with other processes represented in CTMs for the 30 test cases evaluated. Differences between 6M and the discrete model in the mass/volume moment and in the partitioning of sulfur (VI) between the gas and aerosol phases remain under 1% whenever significant aerosol is present, and differences in particle number rarely exceed 15%. Estimates of cloud droplet number from 6M are on average within 16% of those of the discrete model, with a significant part of these differences attributable to limitations of the discrete dynamics. Multimodal lognormal (MIDAS) surrogates to the underlying size distributions derived from the 6M moments are in good agreement with the benchmark size distributions.

1. Introduction

The accurate and efficient representation of aerosol microphysical processes is a growing requirement in the modeling of atmospheric aerosols and their impact on climate, visibility, and air quality. In particular, there is need for a quantitative evaluation of the complex aerosol modules with all the attendant features, simplifications, and necessary approximations that would be used when they are incorporated in regional- to global-scale chemical transport models (CTMs). In this context, evaluations of the complete modules will provide realistic assessments of the expected accuracy and robustness of the aerosol algorithms over a range of meteorological and chemical conditions encountered in the boundary layer and lower troposphere.

1.1. Background

It is becoming increasingly recognized that it is necessary to represent the microphysical properties of aerosols, and not just

the mass of the aerosol, in CTMs and in general circulation models (GCMs) examining aerosol influences on climate. There are two general approaches to this. The traditional approach has been to represent the aerosol size distribution in terms of a probability distribution function $P(r)$, the probability per unit radius interval that a particle has radius r . This approach attempts to represent the evolving particle distribution function (PDF)

$$f(r) dr = NP(r) dr, \quad (1)$$

where $f(r) dr$ is the number of particles per unit volume within the radius range r to $r + dr$ and N is the total number of particles per unit volume. Aerosol properties σ are calculated as integrals of the appropriate radius-dependent kernel function $\sigma(r)$ over the PDF

$$\sigma = \int \sigma(r) f(r) dr. \quad (2)$$

In this approach, the calculation of the evolution of aerosol properties thus requires the explicit calculation of the evolution of the aerosol size distribution.

An alternative approach is to represent the aerosol in terms of the moments of the PDF. The radial moments are defined as

Copyright 2001 by the American Geophysical Union.

Paper number 2001JD900098.
0148-0227/01/2001JD900098\$09.00

$$\mu_k = \int_0^{\infty} r^k f(r) dr, \quad (3)$$

where μ_k is the k th radial moment. In this approach, only the lower order moments are known, and the underlying PDF is unknown. Aerosol properties are derived from the moments by quadrature methods as

$$\sigma = \sum_i \sigma(r_i) w_i, \quad (4)$$

where the sum is taken at radii r_i with weights w_i and where both the r_i and the w_i can be determined from the moments alone. Alternatively, more accurate methods for determining aerosol properties from the moments employ

$$\sigma = \int \sigma(r) g(r) dr, \quad (5)$$

where $g(r)$ is a surrogate for the true PDF derived from the low-order moments [Yue *et al.*, 1997; Wright, 2000] (D. L. Wright *et al.*, Retrieval of aerosol properties from moments of the particle size distribution for kernels involving the step function: Cloud activation, submitted to *Journal of Aerosol Science*, 2000) (hereinafter referred to as Wright *et al.*, submitted manuscript, 2000). In contrast to the PDF approach, the calculation of the evolution of aerosol properties by these latter methods requires the calculation of the evolution of aerosol moments.

1.2. Issues Related to the Use of Moment-Based Aerosol Modeling in CTMs

The method of moments (MOM) potentially offers significant advantages for incorporating aerosol processes in large-scale models provided that closed sets of dynamical equations for evolution of the moments can be obtained [Friedlander, 1983; McGraw and Saunders, 1984; Pratsinis, 1988; McGraw, 1997; Barrett and Webb, 1998]. The advantages of the moment approach include comparatively straightforward implementation of the method as the moments evolve according to sets of differential equations having the same structure as the rate equations describing the evolution of reacting chemical species in the same background flow. Additionally, simulations of aerosol dynamics based on moments are free from the errors associated with numerical diffusion in particle size space, as accurate tracking of the moments, being averages of powers of radius (or volume/mass) over the size distribution, inherently constrains the flow in size space to the specified growth rates. Also, moment-based approaches tend to have much lower computational and storage requirements than are required for explicit and accurate modeling of the PDF itself. There are, however, two important potential limitations to the MOM approach which have largely limited its use in large-scale models. These two limitations, and recent studies on methodologies for overcoming these limitations, are discussed in greater detail below.

The first potential limitation of a moments-based method relates to the fact that exact closure of the moment evolution equations is possible only for highly specialized cases such as free molecular growth [Hulburt and Katz, 1964]. One way of achieving closure is by assumption of a functional form for the PDF, e.g., single or multiple lognormal distributions [Pratsinis, 1988; Whitby and McMurry, 1997]. However, the recently in-

troduced quadrature method of moments (QMOM) allows condensation and coagulation kernels of arbitrary functional form to be treated without a priori assumptions regarding the form of the PDF, and consequently, the QMOM approach has become a viable candidate for modeling aerosols under very general conditions. Here we briefly review previous studies using the QMOM approach and other related moment-based algorithms.

McGraw [1997] treated condensational growth, and Barrett and Webb [1998] treated condensation and coagulation (but not both processes simultaneously) with various quadrature techniques. These first studies established the feasibility of the QMOM for kernels of complex functional form. R. McGraw and D. L. Wright (manuscript in preparation, 2001) extended the QMOM formalism to internally mixed multicomponent aerosols and treated condensation, coagulation, and simultaneous evolution under both processes. That work included a few numerical evaluations using the continuum Brownian kernel; this is a very smooth and nearly constant kernel unless the coagulating particles are of widely disparate sizes. Thus the accuracy of the QMOM for coagulation was exceedingly good in that study, as the MOM is itself exact for the integer volume moments evolving under a constant (size-independent) coagulation kernel. Coagulation with kernels appropriate for particles of all sizes and the formation of new particles were not treated in that study, however. Extension of the QMOM to populations of particles of complex morphology has been achieved with little increase in the computational demands or complexity of the approach [Wright *et al.*, 2001]. In this last study, a bivariate model was developed to represent the dynamics of a population of inorganic nanoparticles undergoing simultaneous coagulation and restructuring. The underlying bivariate PDF employed particle volume and surface area as dynamical variables for parameterization of particles of complex shape [Tandon and Rosner, 1999]. The dynamics represented in that study are quite different from those of atmospheric aerosols.

On a larger scale, a QMOM-based aerosol microphysical module incorporated within a subhemispheric CTM represented nucleation, condensation, coagulation, size-resolved dry deposition, water uptake and release with changing relative humidity (RH), and a rudimentary cloud processing of the aerosol [Wright *et al.*, 2000]. In that study, an external mixture of three different aerosol types was tracked using six moments for each aerosol type.

The second potential limitation of a moments-based method relates to the problem of retrieving aerosol properties of interest from the moments given that the underlying aerosol size distribution is unknown. Several recent studies have addressed this issue. McGraw *et al.* [1995] showed that aerosol optical properties could be obtained directly from six low-order moments using a Gaussian quadrature technique. Yue *et al.* [1997] extended the randomized minimization search technique (RMST) of Heintzenberg *et al.* [1981] to the retrieval of histogram-type representations of the PDF from the moments, from which aerosol properties can be computed. The multiple isomomental distribution aerosol surrogate (MIDAS) technique [Wright, 2000] provides a rapid transformation from moments to smooth model surrogate PDFs (lognormals, modified gammas), which can then be used in the computation of aerosol properties. Aerosol optical properties computed from moments using RMST or MIDAS are typically within 1–2% of those computed directly from the PDF. These techniques are

especially useful when three-point quadrature results in inadequate sampling of the integrands occurring in moment evolution equations or in the estimation of aerosol properties.

Wright et al. (submitted manuscript, 2000) examined the ability of the RMST and MIDAS methods to evaluate integrals over kernels involving the Heaviside step function. Such a step function kernel arises in conjunction with the PM 2.5 air quality standard, where one asks how much of the aerosol has particle diameter less than 2.5 μm , or in the case of cloud activation, where only those particles greater than a critical radius form cloud drops. In each case the computational task involves partitioning the aerosol into two portions based upon some predetermined particle size. This is an especially challenging task for the method of moments, as the moments are integrals over the entire PDF and as such do not contain information about specific portions of the size range. Wright et al. established that moment-based techniques could perform this necessary partitioning to an accuracy of within 10% or better. Retrieval of surrogates ($g(r)$) to the unknown PDF from the moments (as done by RMST and MIDAS) permits more accurate representation of aerosol evolution in clouds than does the simple quadrature-based approach used by Wright et al. [2000].

1.3. Scope of This Study

The present study builds on previous work by evaluating a MOM-based aerosol microphysical model in which all key processes relevant to aerosol evolution are represented for a wide range of environmental conditions. We describe an aerosol dynamical-microphysical module, 6M, based on the QMOM and MIDAS approaches, and explore and evaluate its performance for a range of conditions potentially encountered in the troposphere. Dynamical processes represented include the formation of new particles via binary $\text{H}_2\text{SO}_4\text{-H}_2\text{O}$ nucleation, condensational growth, coagulation, evolution of the aerosol due to cloud processing, size-resolved dry deposition, and water uptake and release with changing RH. These processes are all represented in a zero-dimensional (box) model. It has previously been demonstrated that moment methods employing as many as six moments can be incorporated into three-dimensional (3-D) transport models [Wright et al., 2000], and results of the implementation of 6M in a regional model will be reported elsewhere. The restriction here to a 0-D model (box model) is to test the performance of the module in representing dynamical microphysical processes under conditions that allow comparison with high-resolution PDF model evaluations.

The performance of the moments-based box model is evaluated using results from a high-resolution discrete model of particle dynamics, which serves as a benchmark. The evaluation is restricted to the $\text{H}_2\text{SO}_4\text{-H}_2\text{O}$ aerosol, as evaluation of the treatment of multiple aerosol populations would make excessive computational demands to obtain benchmark results with the discrete model without additionally testing the ability of the module to represent the foregoing processes. The module represents evolution of the six lowest order radial moments, and performance is evaluated primarily by comparison with moments computed from the discrete PDF. Such a comparison is sufficient in view of previous demonstration that aerosol properties can be accurately retrieved from moments.

Thirty test cases have been simulated, each for a period of 30 hours, with a cloud encounter occurring between $t = 8.0$ and $t = 10.0$ hours. The test cases were selected to explore a variety of conditions considering meteorology, initial chemical

concentrations, initial aerosol size distribution, type of cloud encountered, etc. These cases focus specifically on variation of those conditions that directly influence aerosol evolution, rather than being identified as specifically characteristic of continental, marine, or free tropospheric environments, but the conditions selected encompass those typical of tropospheric environments.

Section 2 describes the QMOM, MIDAS, 6M, the discrete model used as the benchmark, and the aerosol processes represented. Section 3 describes the test cases. Section 4 contains results for evolution of the test distributions, evolution of the moments, cloud drop number, and MIDAS surrogates to the PDFs. Section 5 concludes with a perspective on the performance of 6M and further development, some discussion regarding implementation of 6M in a CTM, and a summary.

2. Model Description

2.1. QMOM and MIDAS

2.1.1. Quadrature method of moments. The QMOM is presented and described in detail by McGraw [1997], and its application to coagulation is given by Barrett and Webb [1998]. Using the lowest $2N$ moments ($k = 0\text{--}5$ usually), N quadrature abscissas and weights are determined (via the subroutine ORTHOG [Press et al., 1992]) that satisfy the equations

$$\mu_k = \sum_{i=1}^N r_i^k w_i. \quad (6)$$

These quadrature abscissas and weights are then used to approximate the right-hand side of the moment evolution equations, which have the form

$$\frac{d\mu_k}{dt} = \int_0^\infty \sigma(r) f(r) dr \quad (7a)$$

for “single-particle processes” such as condensation or dry deposition (see equations (10) and (19) below), or

$$\frac{d\mu_k}{dt} = \int_0^\infty \int_0^\infty \sigma(r_1, r_2) f(r_1) f(r_2) dr_1 dr_2 \quad (7b)$$

for “two-particle processes” such as coagulation (see equation (14) below), for the appropriate kernel functions $\sigma(r)$ and $\sigma(r_1, r_2)$. There is no assumption of a functional form for the underlying PDF. The approximation is most accurate with smooth kernels, as occur with condensation and coagulation, and errors are typically under 1% for these processes over significant aerosol evolution. The approximation is exact for kernels of polynomial form provided the degree of the polynomial does not exceed $2N - 1$. The QMOM dynamics is exact for free molecular condensational growth, and for the even-order moments under diffusion-controlled growth [McGraw, 1997]. The quadrature approach can accommodate kernels of arbitrary functional form for condensation, coagulation, dry deposition, wet removal, cloud activation, and other size-dependent processes.

2.1.2. Multiple isomomental distribution aerosol surrogate (MIDAS) method. This technique provides surrogates to the unknown PDF composed of families of smooth multimodal lognormal or modified gamma distributions with each surrogate exactly consistent with $2N$ specified moments. Aerosol

optical properties computed using MIDAS are typically within a few percent of the exact values computed directly from the distribution [Wright, 2000]. Further evaluation (Wright et al., submitted manuscript, 2000) regarding cloud activation for some 240 continental distributions showed that MIDAS could rapidly deliver accurate estimates of particle number and mass for both the interstitial and activating portions of the aerosol, provided the activated number fraction was not extremely small.

2.2. The Module 6M

Most of the core algorithms of 6M were derived from those given by Wright et al. [2000]. Under the assumption that advection and diffusion processes will operate on the dry aerosol in a CTM the various processes in the 0-D box model are performed (with operator splitting) in the following order: primary emissions, water uptake, nucleation-condensation, coagulation, dry deposition, water release, and cloud processing.

For the purpose of the present evaluation, $\text{H}_2\text{SO}_4(\text{g})$ is immediately converted to ammonium sulfate upon incorporation into aerosol particles. Aerosol-water equilibration is assumed to be instantaneous, and water uptake and release are performed with a size-independent water uptake ratio, defined as $\beta_{\text{RH}} = r_{\text{wet}}/r_{\text{dry}}$, computed from the data of Tang and Munkelwitz [1994]. As β_{RH} is size-independent (i.e., the Kelvin effect on the smallest particles is neglected), the moments of the ambient and dry aerosols are related as μ_k (ambient) = $\beta_{\text{RH}}^k \mu_k$ (dry). The aerosol is assumed to be in the metastable (liquid) state whenever the relative humidity is above the efflorescence humidity.

2.2.1. Primary aerosol emissions. Primary (particulate) sulfate emissions are characterized in terms of moments by use of the lognormal distributions given by Whitby [1978] representing a power plant plume, with the normalization determined by the mass emission rate specified by the host 3-D model. Once the source of primary emissions is characterized by source rates of moments, no additional uncertainties are introduced by these source terms during integration of the moment evolution equations.

2.2.2. Nucleation. New particle formation via binary $\text{H}_2\text{O}-\text{H}_2\text{SO}_4$ nucleation is represented using the Jaeger-Voiron and Mirabel [1989] (JVM) model, as parameterized by Fitzgerald et al. [1998], but with a minimum rate of 10^{-6} particles $\text{cm}^{-3} \text{s}^{-1}$ that accounts for nucleation on ions generated by cosmic rays. In grid cells as large as those in regional-to-global models, not only is nucleation expected to be a subgrid process, but it occurs under different conditions in different portions of a cell as meteorological conditions vary throughout the cell. Under different meteorological conditions, nucleation theory predicts that particles of different sizes will form, with the results that in any grid box there will be a distribution of sizes of newly nucleated particles. We represent this underlying but unknown new particle distribution in terms of a three-point quadrature, or tridisperse representation. The nucleated particles are produced at three discrete sizes (r_{N1} , r_{N2} , and r_{N3}) with assumed relative weightings (w_{N1} , w_{N2} , w_{N3} ; $w_{N1} + w_{N2} + w_{N3} = 1$), from which source terms for moments are computed as

$$\frac{d\mu_k}{dt} = J \sum_{i=1}^3 r_{Ni}^k w_{Ni}, \quad (8)$$

where J is the nucleation rate (number $\text{cm}^{-3} \text{s}^{-1}$). (Three sizes are also necessary as a three-point quadrature requires that the underlying distribution be at least tridisperse; inversion from six moments to abscissas and weights can be problematic when the distribution is truly monodisperse or bidisperse.) As previously noted, the neutralization of H_2SO_4 is not explicitly modeled and all H_2SO_4 is treated as ammonium sulfate immediately upon condensation. Specifically, the $\text{H}_2\text{SO}_4(\text{g})$ concentration, temperature, and RH are used to compute the nucleation rate, and the number of new particles formed during the time step is determined. The total condensed dry volume of those particles is then determined using the r_{Ni} and w_{Ni} . Then the molar mass and density of dry $(\text{NH}_4)_2\text{SO}_4$ are used to determine the number of moles of ammonium sulfate contained in that volume, and the $\text{H}_2\text{SO}_4(\text{g})$ concentration is decreased by that amount. Once the nucleation process and rate are specified, the nucleation term (equation (8)) can be calculated exactly.

The uncertainty in the nucleation rate, and even what nucleation process to model, is expected to be one of the greatest sources of uncertainty in modeling the sulfate aerosol. Sensitivity analyses of Raes et al. [1992] and Kreidenweis et al. [1991] suggest that number concentrations can be predicted to within a factor of 1000 during a nucleation burst and a factor of 20 after nucleation has ceased, mostly because of uncertainty in the nucleation rate. Raes and Van Dingenen [1992] employed a nucleation tuner in the range of 10^4 – 10^{-6} and justified it in terms of the uncertainties in the thermodynamic data used to calculate those rates.

2.2.3. Condensational growth. The condensation rate used in 6M is given by the modified Fuchs-Sutugin formula [Russell and Seinfeld, 1998; Hegg et al., 1992; Kreidenweis et al., 1991]

$$\varphi(r) = \frac{dr}{dt} = \frac{v_m DF(Kn) A(Kn)}{r} (\rho^\infty - \rho^{\text{surf}}), \quad (9a)$$

where

$$F(Kn) = \frac{1 + Kn}{1 + 1.71Kn + 1.33Kn^2}, \quad (9b)$$

$$A(Kn) = [1 + 1.33KnF(Kn)(1/\alpha - 1)]^{-1}, \quad (9c)$$

where v_m is the volume of a single ammonium sulfate unit (considering water uptake with RH), D is the diffusion coefficient for $\text{H}_2\text{SO}_4(\text{g})$ in air, ρ^∞ and ρ^{surf} are the $\text{H}_2\text{SO}_4(\text{g})$ concentrations in the bulk vapor and at the surface of the particle, respectively, Kn is the Knudsen number (λ/r), and α is the mass accommodation coefficient. The ρ^{surf} is set to zero as appropriate for sulfuric acid water drops larger than critical cluster size. The temperature and pressure dependence of the diffusion coefficient and mean free path λ are included.

Using the quadrature abscissas and weights, the moment evolution equations become

$$\frac{d\mu_k}{dt} = k \int_0^\infty r^{k-1} \varphi(r) f(r) dr \cong k \sum_{i=1}^3 r_i^{k-1} \varphi(r_i) w_i, \quad (10)$$

where the approximate equality refers to the quadrature. As shown by R. McGraw and D. L. Wright (manuscript in preparation, 2001), the moments evolve under condensational growth solely due to evolution of the abscissas, the weights w_i remaining constant (analogous to the method of characteris-

tics). Thus one may evolve the $r_i(t)$ by integrating $\varphi(r_i) = dr_i/dt$ and use the relation

$$\mu_k(t) \equiv \sum_{i=1}^N [r_i(t)]^k w_i. \quad (11)$$

This is a fortuitous property of the QMOM for condensation: One can integrate a six-parameter (moment) representation of the aerosol by integrating only three variables. As condensation can be a major portion of the computational burden of the model, this is a significant savings.

The loss of sulfuric acid vapor to the aerosol is tracked using mass conservation via

$$\left(\frac{d[\text{H}_2\text{SO}_4]}{dt} \right)_{\text{loss}} = - \frac{1}{v_m} \frac{dV}{dt} \equiv - \frac{4\pi}{v_m} \sum_{i=1}^3 r_i^2 \varphi(r_i) w_i, \quad (12)$$

where $V = 4\pi\mu_3/3$ is the condensed aerosol volume per cm^3 and $[\text{H}_2\text{SO}_4](\text{g})$ is in molecules cm^{-3} . There is also a production term $(d[\text{H}_2\text{SO}_4]/dt)_{\text{production}} = k_{\text{SO}_2}[\text{SO}_2](t)$. The overall time step of the chemistry–aerosol dynamics can be subdivided into any number of substeps, and within each substep the sequence nucleation–condensation is performed.

2.2.4. Coagulation. As particle volumes are conserved during coagulation events, the change in μ_k during a single coagulation event involving a pair of particles is

$$(r_1^3 + r_2^3)^{k/3} - r_1^k - r_2^k.$$

Multiplying this expression by the coagulation rate and integrating over the PDF for both variables gives the evolution equation for the radial moments (see *Barrett and Webb* [1998] for the analogous expression for volume moments)

$$\begin{aligned} \frac{d\mu_k}{dt} &= \frac{1}{2} \int_0^\infty dr_1 \int_0^\infty dr_2 [(r_1^3 + r_2^3)^{k/3} - r_1^k - r_2^k] \beta(r_1, r_2) f(r_1) f(r_2), \\ & \quad (13) \end{aligned}$$

where $\beta(r_1, r_2)$ is the coagulation rate. The three-point quadrature approximation to (13) is

$$\frac{d\mu_k}{dt} \equiv \frac{1}{2} \sum_{i=1}^3 \sum_{j=1}^3 [(r_i^3 + r_j^3)^{k/3} - r_i^k - r_j^k] \beta(r_i, r_j) w_i w_j. \quad (14)$$

The Fuchs kernel [*Fuchs*, 1964; *Jacobsen et al.*, 1994], valid over the full range of particle size, is used via a lookup table interpolation that is accurate to within 0.05%.

2.2.5. Cloud processing. Aerosols have important impacts on cloud properties such as enhancing cloud albedo and the “indirect effect” of aerosol forcing of climate. Conversely, clouds have important effects on aerosol evolution. The accumulation mode is almost entirely responsible for aerosol optical properties and is thought, at least in the marine boundary layer, to be itself largely the result of repeated cycles of aerosol growth within nonprecipitating clouds [*Hoppel et al.*, 1994]. It is also likely that wet removal via precipitation dominates dry deposition as a sink for sulfate aerosol to a significant extent [*Slinn*, 1983]. Thus it is important to model the effect of clouds

on aerosols, as well as the effect of aerosols on cloud optical and radiative properties.

Our primary concern here is to model the evolution of the aerosol due to its encounter with clouds in a CTM. Although in the subsequent discussion we will be concerned with estimating cloud drop number, one must bear in mind that the primary reason for doing so is to evolve the aerosol moments accurately. Should the model provide useful predictions of cloud drop number N_c , such predictions would be an added bonus beyond the primary objectives of a CTM. The ability of a CTM with a representation of aerosol microphysics to provide estimates of cloud properties, such as cloud drop number, is strictly a matter beyond the fundamental reach of such models.

In principle, clouds are dynamically evolving, although this is not yet well represented in large-scale models. Evolution of supersaturation with time, including the feedback of the aerosol and the growing cloud droplets on that supersaturation, has been modeled in detailed studies of cloud physics, but cloud nucleation remains highly parameterized in large-scale models such as GCMs [*Ghan et al.*, 1997; *Abdul-Razzak et al.*, 1998].

In a CTM such cloud evolution is not modeled. Rather, at each time step and grid cell the meteorological driver provides a number of parameters specifying the state of the air. Key parameters are cloud type and quantities such as fractional cloud cover, liquid water content (LWC), and vertical velocity. When the meteorological driver indicates that cloudy air is present, the aqueous chemistry routine typically uses LWC, gas phase SO_2 concentration, Henry’s law, and oxidant concentrations to calculate the total amount of sulfate produced per unit volume of cloudy air. The cloud drops in which this chemistry has taken place had formed around aerosol particles, and these particles retain the sulfate produced there. In view of the extreme narrowing of cloud drop size distributions relative to the size distribution of the activated particles, and because aqueous reaction rates within clouds are, to good approximation, proportional to cloud drop volume, we approximate the apportioning of sulfate formed by aqueous phase reactions by distributing this material equally among the activated particles. Thus once one has an estimate of cloud drop number, each activated aerosol particle accretes the same, known amount of sulfate mass.

When cloud is formed in an air parcel, the method of moments (MOM) must partition the aerosol into activating and interstitial portions and characterize each portion by a set of moments. (The zeroth moment of the activating portion will give N_c .) This poses a unique problem for the MOM not encountered with the other dynamic processes considered. This partitioning must be done using only the moments and without other information regarding the PDF, yet the partitioning implicitly requires that knowledge of two distinct portions of the size spectrum be obtained from moments that are integral quantities over the full size range of the PDF. Though it would seem that the moments do not carry the requisite information to accomplish this feat, this has proved to be a tractable problem. The module 6M performs this partitioning (thereby estimating N_c), performs scavenging of the interstitial aerosol by cloud drops, and apportions sulfate mass among the cloud drops. We outline the steps involved to implement this moment evolution in cloudy air.

2.2.5.1. Step 1: An estimate of cloud droplet number is obtained. This is done using the aerosol activation model of *Abdul-Razzak et al.* [1998], which implicitly accounts for con-

trol of maximum supersaturation by aerosol concentration and size distribution. For a single aerosol type this model requires representation of the aerosol PDF in terms of a lognormal distribution. The lognormal parameters N , r_g , and σ_g can be obtained algebraically from any three of the six moments: μ_0 , μ_1 , and μ_3 are used here. These parameters and meteorological variables are used by the activation model to estimate the activated fraction (N_c/N) of the aerosol. Activated fraction and particle number ($N = \mu_0$) together yield an estimate of cloud droplet number.

2.2.5.2. Step 2: A MIDAS surrogate to the unknown PDF is retrieved from the six moments. This surrogate is integrated from infinity down to $r_{c,\text{eff}}$, where $r_{c,\text{eff}}$ is the particle radius such that integration of the surrogate PDF from $r_{c,\text{eff}}$ to infinity yields a number of particles equal to the cloud droplet number estimated in step 1. Thus $r_{c,\text{eff}}$ is taken as the particle size at which to partition the surrogate PDF into activating and interstitial portions. The surrogate PDF, multiplied by r^k , is then integrated from 0 to $r_{c,\text{eff}}$ to obtain the moments of the interstitial aerosol, $\mu_{k,\text{inter}}$. Subtracting these moments from the total moments yields the moments of the activating portion of the aerosol, $\mu_{k,\text{act}}$.

The modified-gamma version of the MIDAS method [Wright, 2000] is currently enabled in 6M for computing the moments of the interstitial aerosol. Should a set of moments arise for which the modified-gamma retrieval is unsuccessful, a retrieval using lognormals is used. In the case that the MIDAS surrogate has extremely narrow modes either the activating or interstitial portions of the aerosol could be effectively (as far as ORTHOG is concerned) less than tridisperse, leading to problems in subsequent quadratures; in this case the activated fraction computed in step 1 is applied to particle number only, with the normalized higher moments of both portions of the aerosol being the same.

2.2.5.3. Step 3: Scavenging of the interstitial aerosol by cloud drops is now performed via Brownian coagulation between the interstitial aerosol and N_c cloud drops. A three-point quadrature is first performed using the moments of the interstitial aerosol, yielding a set of quadrature abscissas $\{r_i\}$ and weights $\{w_i\}$ that are interpreted as a tridisperse surrogate to the interstitial PDF. Each of these particle sizes is scavenged through coagulation with the N_c cloud drops. The cloud drop size distribution is approximated as monodisperse with a drop radius R_c estimated using cloud LWC. For the tridisperse interstitial aerosol the particle number of each size is reduced according to

$$\frac{dw_i}{dt} = -\beta(r_i, R_c)w_iN_c, \quad (15)$$

where $\beta(r_i, R_c)$ is the coagulation rate computed from the Fuchs kernel. For evolution over a time step Δt this equation integrates to

$$w_i(t + \Delta t) = w_i(t) \exp[-\beta(r_i, R_c)N_c\Delta t]. \quad (16)$$

The sulfate mass acquired by cloud drops during this scavenging is tracked for use in the following step. Coagulation within the interstitial aerosol itself was not performed in these simulations (but could be readily added), nor was drop coalescence.

2.2.5.4. Step 4: Sulfate mass is now added to the activated particles. This sulfate includes the mass produced by the aqueous chemistry during the time step, the mass acquired through scavenging of the interstitial aerosol, and the mass in

the gas phase as $\text{H}_2\text{SO}_4(\text{g})$, as it is assumed that cloud drops capture any $\text{H}_2\text{SO}_4(\text{g})$ present. The sulfate mass is added by performing a three-point quadrature on the $\mu_{k,\text{act}}$ yielding three discrete particle sizes $\{r_i\}$ and their relative weights, with the total number of particles equal to $N_c = \mu_{0,\text{act}}$. Each of these particles is given an equal portion of the sulfate, and the abscissas are updated according to

$$r_i(t + \Delta t) = r_i(t)[1 + \Delta m/m_i]^{1/3}, \quad (17)$$

where m_i is the mass contained in a particle of (dry) radius r_i and Δm is the sulfate mass gained by each cloud drop. The $\mu_{k,\text{act}}$ are then updated by computing them from the updated abscissas and (unchanged) weights.

2.2.5.5. Step 5: After evolution of the interstitial aerosol in step 3 and of the activated aerosol in step 4 the moments of these two portions of the aerosol are summed to give the moments of the full in-cloud aerosol at the end of the time step. A potential problem that may arise is that the meteorological driver may specify that a cloud exists while the aerosol dynamics may simultaneously specify that few or no aerosol particles are present to form cloud drops. In the paper by Wright *et al.* [2000], if the meteorological driver indicated that a cloud was present and the aerosol did not provide at least 100 cloud drops, then 100 initially massless particles were inserted to receive the sulfate mass produced by the aqueous chemistry. An approach such as this seems unavoidable in models with a mixture of externally driven and dynamically evolved aerosols and clouds. However, no such instances arose in the test cases reported here.

2.2.6. Dry deposition. Deposition velocity varies considerably with particle size, and aerosol deposition is treated as size-dependent. For the evolution of the PDF,

$$\frac{df(r)}{dt} = -\frac{v_d(r)}{\Delta z}f(r) = -\psi(r)f(r), \quad (18)$$

where $v_d(r)$ is the deposition velocity (which also depends on wind speed) and Δz is the height of the lowest vertical layer in the model. This equation has the solution $f(r, t) = f(r, 0) \exp[-\psi(r)t]$, and the moments evolve according to

$$\begin{aligned} \mu_k(t + \Delta t) &= \int_0^\infty r^k f(r, t + \Delta t) dr \\ &= \int_0^\infty dr r^k f(r, t) e^{-\psi(r)\Delta t} \cong \sum_{i=1}^3 r_i^k w_i(t) e^{-\psi(r_i)\Delta t} \\ &= \sum_{i=1}^3 r_i^k w_i(t + \Delta t), \end{aligned} \quad (19)$$

which shows that after an initial quadrature the moments evolve during the time step through evolution of the weights alone according to $w_i(t + \Delta t) = w_i(t) e^{-\psi(r_i)\Delta t}$ with the abscissas remaining constant. As in the marine boundary layer model of Fitzgerald *et al.* [1998], the deposition velocities have been calculated from the model of Giorgi [1986] for deposition to both ocean and land surfaces.

2.3. Discrete Model of Particle Dynamics

2.3.1. General features. To evaluate the performance of 6M, we have computed benchmark results using a high-

resolution discrete representation of the PDF. For each process represented by 6M the appropriate term of the aerosol general dynamic equation was integrated by the discrete scheme, with operator splitting as in 6M. A fixed logarithmic scale in radius was used and extended far enough to insure that the distribution amplitude is negligible at the large- r end of the spectrum. This was checked by monitoring convergence of μ_5 (the highest moment needed and the one most sensitive to the tail of the PDF) as the discrete PDF is integrated out to large r . These results were obtained using 500 grid points spanning the range of dry radius 0.001–20 μm . Much of the process description given above applies to the discrete model as well as to 6M. This discrete model was derived from the one used by R. McGraw and D. L. Wright (manuscript in preparation, 2001) and *Wright et al.* [2001].

2.3.2. Nucleation. To facilitate comparison, new particle formation is performed in precisely the same manner as in 6M, and at the same three particle sizes. Thus, for any simulation of nucleation only, 6M and the discrete model obtain the same results. As noted in section 2.2.2, integration of the nucleation term of the moment evolution equations introduces no additional uncertainties in the moments other than those inherent in the choice of nucleation process and the representation of the nucleation rate.

2.3.3. Condensational growth. During each integration substep each of the N_i particles of radius r_i grows by dr_i such that $r_{\text{NLO}} < r_i + dr_i < r_{\text{NHI}}$, where r_{NLO} and r_{NHI} are the radii of the two neighboring grid points NLO and NHI, respectively. The total volume contained in the N_i particles of radius $r_i + dr_i$ is apportioned between neighboring grid points NLO and NHI such that total volume and number are conserved. Condensation tends to suffer more from numerical diffusion than does coagulation, as is known from efforts to accurately model condensation using a fixed-bin sectional approach. Previous comparisons of results from this grid scheme for condensational growth (unpublished) with results from the method of characteristics (exact) showed good agreement for the μ_k when sufficiently high grid resolution (1000 or more grid points) is used.

2.3.4. Coagulation. For N coagulation events between particles of radii r_i and r_j (grid points i and j) during an integration step, N particles of radius $r_k = (r_i^3 + r_j^3)^{1/3}$, with $r_{\text{NLO}} < r_k < r_{\text{NHI}}$, are obtained, with N particles each of radii r_i and r_j lost in the process. The material contained in the N particles of radius r_k is apportioned between grid points NHI and NLO such that the number of new particles N and the total volume $N(4\pi/3)r_k^3$ are each conserved during the apportionment. This is done by simultaneously solving the equations $N = N_{\text{NLO}} + N_{\text{NHI}}$ and $Nr_k^3 = N_{\text{NLO}}r_{\text{NLO}}^3 + N_{\text{NHI}}r_{\text{NHI}}^3$ for N_{NLO} and N_{NHI} , the increments to be added to the numbers of particles at grid points NLO and NHI, respectively. Previous comparison of this algorithm with the finite element method (FEM) results of *Barrett and Webb* [1998] showed good agreement between the two approaches when their low-order moments were compared. Exact solutions for the integer volume moments, available from the method of moments (MOM) for constant kernel coagulation, provide an important test of this model as it is the accuracy of the moments of the discrete scheme that is most relevant for this work. Numerical results for the constant kernel moments obtained by integrating the discrete model PDF (unpublished) were found to be in excellent agreement with exact moments obtained from the MOM.

2.3.5. Cloud processing. As in 6M, the discrete model partitions the aerosol into activating and interstitial portions, performs scavenging of the interstitial aerosol by cloud drops, and apports sulfate mass among the activated particles. Analogous to 6M, the discrete model performs the following steps.

2.3.5.1. Step 1: The activated fraction and cloud drop number are computed as in step 1 for 6M except that moments computed from the discrete PDF are used in determining the lognormal parameters required by the activation model and integration over the PDF rather than moment-based surrogates is used.

2.3.5.2. Step 2: The grid is partitioned into interstitial and activating portions by allowing the largest $N_{c,\text{discrete}}$ particles to activate. For computational convenience each grid point is classified as activating or interstitial, and the number of grid points that activate is determined as the minimum number that will yield $N_{c,\text{discrete}}$ at least as great as N_c . This results in slight overestimation of N_c . The significance of this overestimation at a resolution of 500 grid points was assessed using a few additional runs at resolutions of 1000 and 2000 points and is described in section 4.

2.3.5.3. Step 3: Scavenging of the interstitial aerosol is performed via Brownian coagulation according to (15) and (16) with w_i in those equations replaced by N_i , the number of particles at each point i of the interstitial portion of the grid.

2.3.5.4. Step 4: Each activated particle receives an equal portion of the sulfate mass derived from aqueous chemistry, scavenging, and $\text{H}_2\text{SO}_4(\text{g})$. As activated particles of size i grow to a size that does not correspond to a grid point, conservation of particle number and mass are treated in like manner to their treatment during condensation and coagulation.

2.3.6. Dry deposition. The discrete model is exact at any resolution for this process. The particle number N_i of grid point i is reduced each time step Δt according to

$$N_i(t + \Delta t) = N_i(t) \exp[-\psi(r_i)\Delta t], \quad (20)$$

with $\psi(r_i)$ defined by (18).

3. Test Cases

All test cases represented nucleation, condensation, coagulation, and cloud processing; dry deposition is enabled only when noted. In each case, cloudy air is present during between $t = 8.0$ and $t = 10.0$ hours only. The overall time step was 0.1 hour for both models, although many of the algorithms in both models divide the overall time step into a number of substeps in one way or another. Consistency with the discrete model required that only one substep per time step be used in 6M in the treatment of coupled nucleation and condensation (see section 2.2.3). This 6-min time step for nucleation-condensation is probably adequate in our test cases except when the nucleation rate is very large ($>100 \text{ cm}^{-3} \text{ s}^{-1}$) near the beginning of a few of the cases. Primary emissions have not been included in the simulations reported in section 4; integration of these terms introduces no errors in the moments, and the presence of these terms would only tend to mask errors arising from other terms for which 6M needs to be evaluated.

For these evaluations the (dry) radii of nucleated particles were taken as $(r_{N1}, r_{N2}, r_{N3}) = (2 \text{ nm}, 3 \text{ nm}, 5 \text{ nm})$ and $(w_{N1}, w_{N2}, w_{N3}) = (0.4, 0.5, 0.1)$ for both models (see section 2.2.2). The (JVM) nucleation function is most appropriate for

Table 1. Test Cases^a

Test Case	Dry Deposition	Cloud Type	Initial Aerosol			Initial Concentrations	
			$N_{0,3}$ cm ⁻³	r_g , μm	σ_g	$[\text{H}_2\text{SO}_4]_{0,3}$ mol cm ⁻³	$[\text{SO}_2]_{0,3}$ mol cm ⁻³
1–3	none	cumulus	0	0	0	0	0
4–6	none	cumulus	100	0.01	2.0	0	0
7–9	none	stratiform	100	0.01	2.0	0	0
10–12	none	stratiform	100	0.01	2.0	5.0×10^{-15}	1.0×10^{-12}
13–15	none	cumulus	100	0.01	2.0	5.0×10^{-15}	1.0×10^{-12}
16–18	none	cumulus	0	0	0	5.0×10^{-15}	1.0×10^{-12}
19–21	to land ($W = 5.0 \text{ m s}^{-1}$)	cumulus	0	0	0	5.0×10^{-15}	1.0×10^{-12}
22–24	to ocean ($W = 10 \text{ m s}^{-1}$)	stratiform	100	0.01	2.0	5.0×10^{-15}	1.0×10^{-12}
25–27	none	stratiform	100	0.10	2.0	5.0×10^{-15}	1.0×10^{-12}
28–30	none	stratiform	1000	0.10	2.0	5.0×10^{-15}	1.0×10^{-12}

^aInitial aerosol number N_0 , initial lognormal geometric mean radius r_g , and initial $\text{H}_2\text{SO}_4(\text{g})$ and $\text{SO}_2(\text{g})$ concentrations. W is the 10-m wind speed. Cases are grouped in sets of three, with the first member in each set using meteorology 1, the second using meteorology 2, and the third using meteorology 3.

slightly smaller sizes, but the very rapid relative growth of very small particles poses excessive computational demands on the discrete model (although not on the QMOM). During condensation the mass accommodation coefficient in (9c) is set to unity.

Three meteorological scenarios were selected, each scenario more favorable to nucleation than the preceding one:

Meteorology 1 $T = 298.15 \text{ K}$, $\text{RH} = 50\%$,

Meteorology 2 $T = 298.15 \text{ K}$, $\text{RH} = 80\%$,

Meteorology 3 $T = 270.15 \text{ K}$, $\text{RH} = 95\%$.

These RH values apply when clouds are not present. For all cases, $p = 1 \text{ atm}$.

A constant source rate of SO_2 at $1.0 \times 10^{-13} \text{ mol h}^{-1}$ is assumed. The first-order rate constant for gas phase oxidation of SO_2 to H_2SO_4 is set at $k_{\text{SO}_2} = 6.0 \times 10^{-7} \text{ s}^{-1}$.

In cloud a constant source rate of $\text{H}_2\text{SO}_4(\text{aq})$ of $1.0 \times 10^{-14} \text{ mol cm}^{-3} \text{ h}^{-1}$ is assumed, implying a loss rate of SO_2 of the same magnitude. Details of the in-cloud aqueous chemistry are not modeled. For cumulus (stratiform) clouds an updraft velocity of 500 (50) cm s^{-1} and a liquid water content of 0.60 (0.25) g m^{-3} are assumed. When dry deposition to land (ocean) is enabled, the 10-m wind speed W is set to 5.0 (10.0) m s^{-1} .

The 30 test cases are grouped in sets of three, according to the meteorological conditions described above, and are used in the order 1-2-3 within each set. Each set is characterized with initial concentrations of aerosol and chemical species, the type of cloud to be formed, and the conditions of dry deposition, when enabled. A description of each test case is given in Table 1.

4. Results

Figure 1 shows the initial (if present) and final normalized distributions from the discrete model for each test case as equal-area plots, $dN/d \log_{10} r$ versus $\log_{10} r$. There is substantial aerosol evolution in each test case. The final distributions are always rather narrow, as condensational growth tends to narrow distributions of small particles. In a Eulerian model, aerosol samples from many cells with different environmental conditions are mixed, typically resulting in broader distribu-

tions than the final distributions shown here. This figure shows that the test cases encompass a range of scenarios including evolution to narrow distributions and evolution to multimodal distributions.

4.1. Comparisons of 6M and the Discrete Model

Fractional differences (percent) in the 6M and discrete model results for quantity Q are defined as $\{100\% \times [Q(6M) - Q(\text{discrete model})]/Q(\text{discrete model})\}$. For each test case, fractional differences in the 6M and discrete model moments were saved at the beginning of each model hour, and the maximum magnitude among those 30 values is shown in Figure 2.

Of the six moments tracked, the mass/volume moment μ_3 generally shows the smallest differences with the discrete results, which do not exceed 1% except in the first hours of cases 1 and 2, where almost all of the sulfur (VI) is still in the gas phase. These are differences in partitioning the sulfur (VI) between the gas and aerosol phases, and in all cases 6M tracks the total sulfur (VI) (aerosol phase plus gas phase) to within 0.1% unless a removal process such as dry deposition is enabled.

Differences in particle number μ_0 seldom exceed 10% before the cloud encounter, or 15% after cloud evaporation. These differences are small compared to uncertainties in the nucleation rate that primarily determines number concentrations.

The greatest differences in the 6M and discrete results typically occur in the highest moments (μ_4 and μ_5), especially upon cloud evaporation. These moments are the most difficult to model and evaluate, as they are very sensitive to the tail of the distribution and to any numerical diffusion in the distribution model used to evaluate the performance of 6M. In cases 11–15, 17, 20, and 23 the peak differences in μ_5 reach -25 to -40% upon cloud evaporation, and only in cases 6, 9, and 10 did the peak differences reach -40 to -80% . These latter three cases are instances in which the MIDAS surrogates were very narrow, and therefore the aerosol was not partitioned into activated and interstitial portions in a size-resolved manner (see section 2.2.5). The lack of size-resolved treatment in such cases most strongly impacts the higher moments, and possible reasons for the signs of these errors are discussed in section 4.2.1. In each of the cases cited here, these differences in μ_5

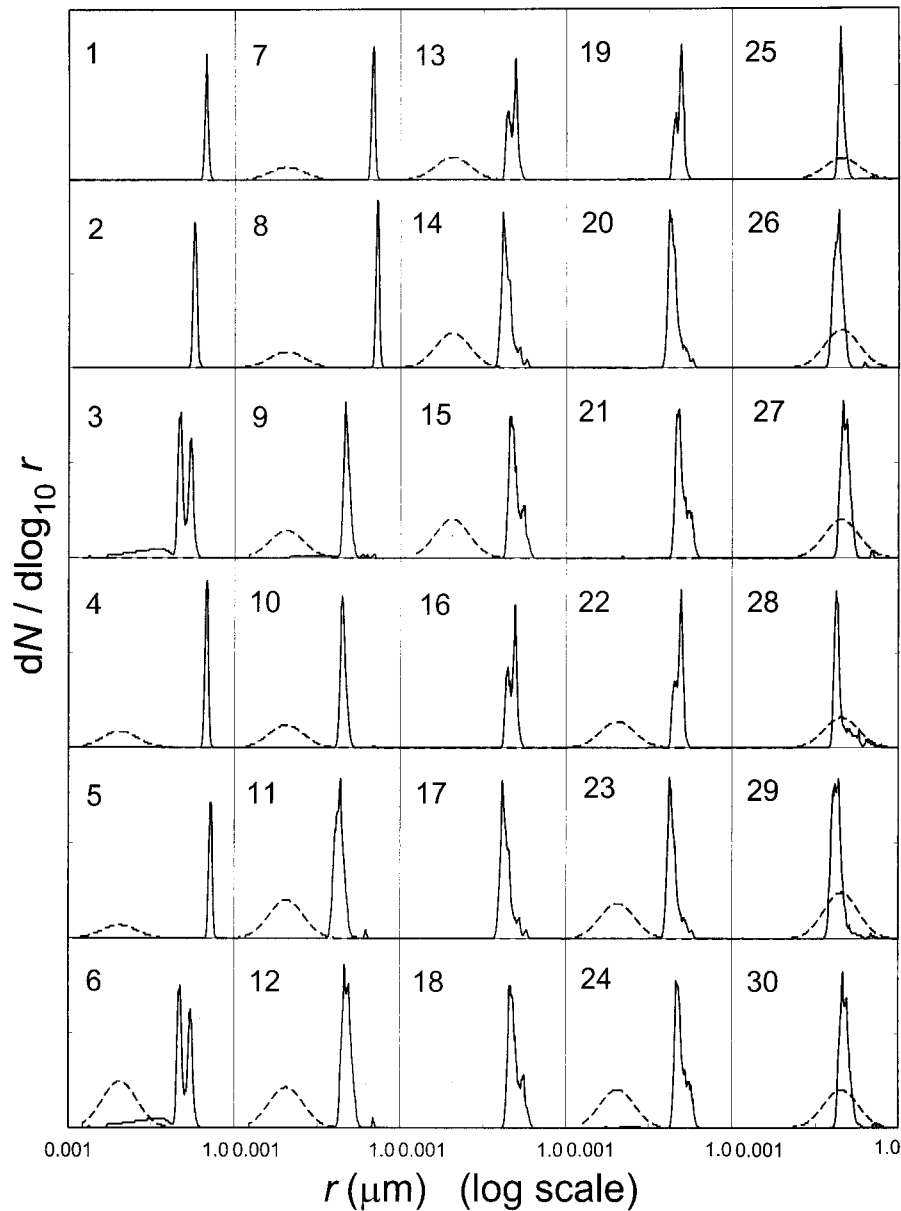


Figure 1. Initial (dashed lines) and final (solid lines) normalized distributions (at ambient RH) for each test case from the discrete model. All distributions are plotted as equal-area plots, $dN/d \log_{10} r$ versus $\log_{10} r$. In each panel the distributions have been scaled to allow the plots to fill the panel vertically.

diminished to about half their peak values by the end of the simulations. We note that μ_5 itself increased by 5–10 orders of magnitude over the simulated time period.

Before detailing some selected cases that were most challenging to 6M, we make a few remarks on cases in which 6M performed especially well. In cases 1, 2, 4, 5, 7, and 8, particle number remained under 800 cm^{-3} , usually under 150 cm^{-3} , with the result that almost all particles activated to form cloud drops, leaving no interstitial aerosol. Differences in the 6M and discrete moments remained under a few percent in these cases as differences associated with the scavenging of interstitial particles were absent. Cases 25–27 and 28–30 have initial conditions as in cases 10–12 except that substantially greater amounts of preexisting aerosol were present. The 6M–discrete model differences in these last six cases were on the whole

about the same as those obtained in cases 10–12, and the heavy initial aerosol loadings posed no special difficulties.

4.2. Detailed Discussion of Selected Cases

Figures 3 and 4 show moment evolution obtained from 6M and the discrete model, along with the fractional differences in the 6M–discrete model moments, for cases 3, 6, 9, 12, 15, and 18. These cases were selected for more detailed discussion as each represents aerosol evolution under meteorology 3, the most favorable of the test meteorologies to new particle formation and that providing the greatest modeling challenge. The 6M–discrete model differences in these cases are almost always larger than those in the analogous cases with meteorology 1 or 2.

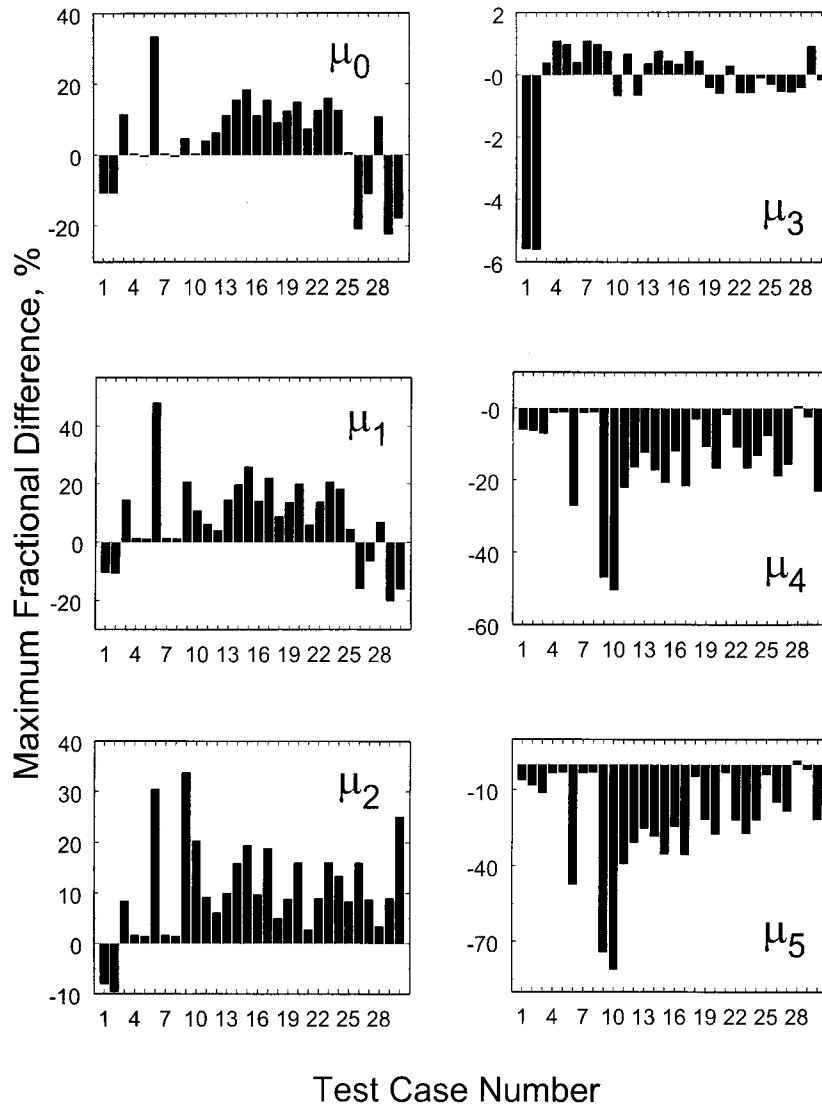


Figure 2. Maximum fractional differences (percent) between the moments of the discrete model and those of 6M over the 30 hours of each test case. For each test case, fractional differences were saved at the beginning of each model hour, and the maximum magnitude among those 30 values is shown here. (Note that Figures 3 and 4 use data recorded every 0.1 hour, as additional data were obtained for the six cases represented in those figures.)

4.2.1. Case 3. Aerosol evolution in case 3 begins with no aerosol or vapor species present. A nucleation burst begins around $t = 0.5$ hours, with the number concentration rising to its peak value of $21,000 \text{ cm}^{-3}$ at $t = 2.0$ hours, followed by a slow nucleation rate ($0.001\text{--}0.1 \text{ cm}^{-3} \text{ s}^{-1}$) throughout the remainder of the simulation. By the time of cloud formation at $t = 8.0$ hours, coagulation has reduced particle number to $15,600 \text{ cm}^{-3}$. During this period of rapid coagulation and moment evolution, differences in the 6M–discrete model moments μ_0 , μ_1 , μ_2 , μ_3 , μ_4 , and μ_5 remain under 0.5, 0.9, 0.8, 0.1, 1.5, and 3.6%, respectively, indicating the ability of the QMOM to track moment evolution under coagulation, as well as the ability of 6M to track simultaneous nucleation, condensation, and coagulation.

In case 3, cloud drop number is initially 86 cm^{-3} in 6M and 261 cm^{-3} in the discrete model, both values rising and leveling off around 3000 cm^{-3} at $t = 9.0$ hours. The time-averaged N_c

over the cloud lifetime for the two models is 2423 cm^{-3} (6M) and 2656 cm^{-3} (discrete model). Comparison of these values with the total particle number during the cloud lifetime indicates that substantial interstitial aerosol is present, and scavenging of the interstitial aerosol reduces particle number from $15,600$ to $\sim 8,500 \text{ cm}^{-3}$ upon cloud evaporation at $t = 10$ hours. At this time, differences in the 6M–discrete model moments reach values of 12, 14, 8, 0.01, 7, and 11%, which are maximum differences in all moments except μ_3 . (Differences in μ_3 are reduced by cloud formation as all $\text{H}_2\text{SO}_4(\text{g})$ is taken into the aerosol, and prior errors in gas-aerosol partitioning are thereby corrected. Also, mass is tracked exactly by the cloud processing algorithm.) As the 6M–discrete model differences are usually greatest immediately following a cloud encounter, and the reasons are similar in most cases, we give further results during the cloud lifetime for this case.

In case 3, at the first time step the cloud is present the

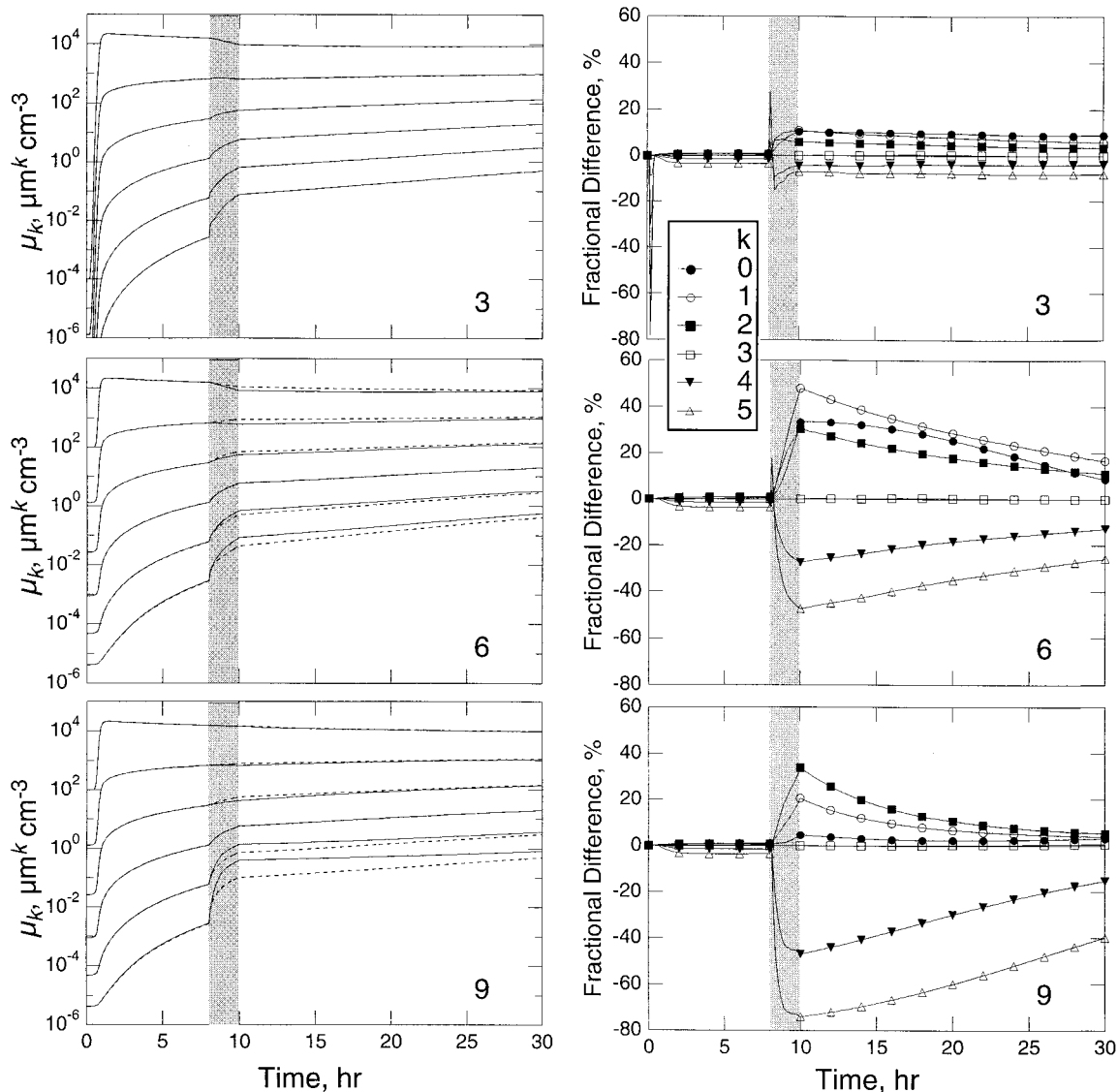


Figure 3. (left) Time evolution of the radial moments (μ_k , $k = 0-5$) of the sulfate aerosol (at ambient RH) for cases 3, 6, and 9 from the discrete model (solid lines) and from 6M (dashed lines). (right) Corresponding percent differences in the 6M moments. Shaded regions between $t = 8.0$ and $t = 10.0$ hours indicate the presence of clouds. Moment k has units of $\mu\text{m}^k \text{cm}^{-3}$.

lognormal parameters obtained for input into the activation model [N (cm^{-3}), r_g (μm), σ_g] are [15,690, 0.01918, 1.1486] in 6M and [15,640, 0.01901, 1.1741] in the discrete model, giving activated fractions of 0.00549 and 0.0130 (overestimated as 0.0167 with 500 grid points), respectively. These activated fractions yield $N_c = 86.1 \text{ cm}^{-3}$ and $N_c = 261.4 \text{ cm}^{-3}$ in 6M and the discrete model, respectively. The difference in values of N_c is due in part to the sensitivity of the activation model to σ_g when the distribution is narrow (see Figure 5 of *Abdul-Razzak et al.* [1998]) and is implicitly a sensitivity to those moments used to determine σ_g . The difference in N_c values is also due in part to the overestimation of activated fraction with the limited resolution of the discrete model (500 grid points). Additional runs for this case were made at resolutions of 1000 and 2000 points. The results for N_c at $t = 8.0$ hours with 500, 1000, and 2000 points were 261.4, 152.4, and 103.7 cm^{-3} , respec-

tively, with the discrete results evidently approaching the 6M value of 86.1 cm^{-3} .

As discussed in section 2.2.5, when cloud activation occurs in the model when the underlying distribution is very narrow, MIDAS can often only retrieve narrow lognormals, and in such situations the activated fraction is applied to particle number only, and the higher normalized moments are the same for both the activated and interstitial aerosols. This implies that cloud activation in these cases is not treated in a size-resolved way, i.e., larger particles are not preferentially activated. This lack of size resolution results in implicit overscavenging of larger particles, as there are now larger particles present in the interstitial aerosol, and underscavenging of smaller particles, as some fraction of the smaller particles are not treated as interstitial. This may account for the fact that μ_4 and μ_5 , which are very dependent upon the larger particles, are usually

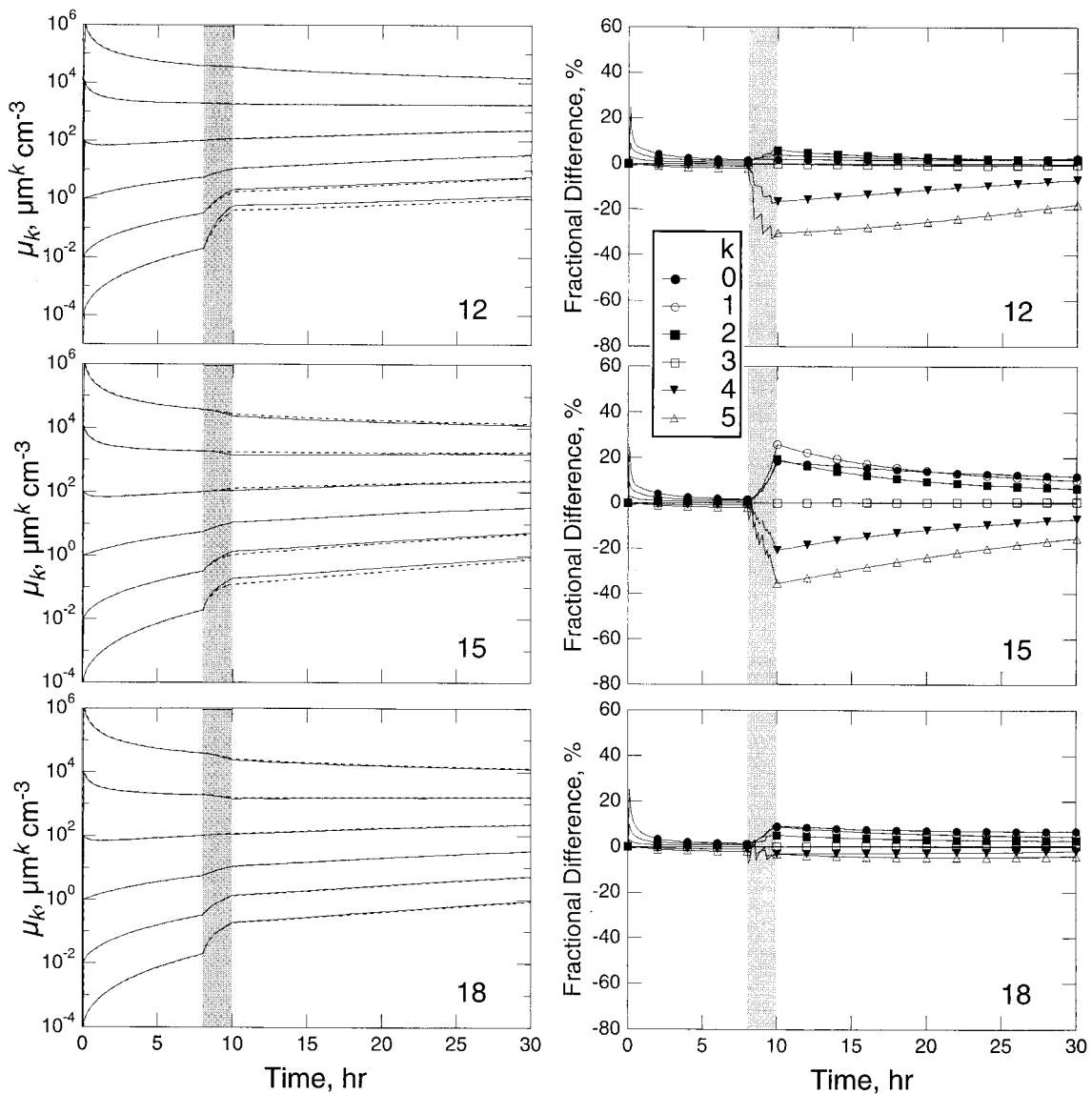


Figure 4. Same as Figure 3, except for cases 12, 15, and 18.

too low in 6M upon cloud evaporation. It is also possible that numerical diffusion in the discrete model accounts in part for this, since such diffusion results in overestimation of these moments in a distribution model.

Differences in the 6M–discrete model moments resulting from cloud encounters are also due to inaccuracies in modeling the coagulation rates of interstitial particles with cloud drops. Such inaccuracies are due to the fact that the rate of Brownian coagulation of small particles with the much larger cloud drops is more strongly size-dependent than coagulation among particles of similar size. This sharper size dependence contributes to the larger errors in 6M Brownian coagulation scavenging than those that occur in its treatment of coagulation among aerosol particles, where accurate results are usually obtained, as during the first 8 hours of case 3 (and case 12 discussed in section 4.2.3).

4.2.2. Cases 6 and 9. Cases 6 and 9 begin with aerosol present ($100 \text{ particles cm}^{-3}$) but no vapor species, with cumulus and stratiform clouds encountered again between $t = 8.0$

and $t = 10.0$ hours, respectively. Moment evolution before cloud formation is identical in these two cases, and quite similar to that in case 3, as the initial aerosol present in these cases is insufficient to greatly impact the formation of new particles. In cases 6 and 9, particle number just before cloud formation is $15,500 \text{ cm}^{-3}$.

In case 6, N_c in 6M begins at 110 cm^{-3} and peaks at 2350 cm^{-3} . In the discrete model, N_c begins at 283 cm^{-3} and peaks at 3320 cm^{-3} . The time-averaged N_c for the two models is 1906 cm^{-3} (6M) and 2668 cm^{-3} (discrete model). Scavenging of the interstitial aerosol reduces particle number to $11,200 \text{ cm}^{-3}$ (6M) and 8400 cm^{-3} (discrete model) upon cloud evaporation. In this case, the apparent underestimation of N_c by 6M results in less scavenging of the interstitial aerosol, with the result that particle number is 33% too high after cloud evaporation. As in case 3, the cloud activation was not size-resolved in 6M, and μ_4 and μ_5 are again too low after the cloud event.

Case 9 yielded the largest 6M–discrete model difference in average N_c found in any of the test cases, with average N_c

Table 2. Cloud Drop Number at $t = 8.0$ Hours and Time-Averaged Cloud Drop Number, for Cases 3 and 9, From Various Models Used in This Study

Model	Cloud Drop Number N_c , cm^{-3}	
	$t = 8.0$ Hours	Time-Averaged
<i>Case 3</i>		
Discrete with 500 points	261.4	2657
Discrete with 1000 points	152.4	2606
Discrete with 2000 points	103.7	2545
6M	86.1	2423
<i>Case 9</i>		
Discrete with 500 points	103.3	168.4
Discrete with 1000 points	83.7	155.7
Discrete with 2000 points	78.9	148.8
6M	78.0	82.0

values of 82 cm^{-3} (6M) and 168 cm^{-3} (discrete model), partly a result of the typically smaller cloud drop number in stratiform clouds. As in case 3, additional discrete model runs were made at resolutions of 1000 and 2000 grid points. The results for N_c at $t = 8.0$ hours with 500, 1000, and 2000 points were 103.3, 83.7 and 78.9 cm^{-3} , respectively, with the discrete results converging to the 6M value of 78.0 cm^{-3} . When compared with the 1000- and 2000-point discrete results, the lower 6M moments were more accurate, but the higher moments were less accurate, than when compared with the 500-point results. Table 2 summarizes the N_c values (at $t = 8.0$ hours) from 6M and the discrete model at various resolutions for cases 3 and 9.

4.2.3. Cases 12 and 15. The initial conditions in cases 12 and 15 are the same as those in cases 9 and 6, respectively, except that cases 12 and 15 have substantial initial concentrations of $\text{SO}_2(\text{g})$ and $\text{H}_2\text{SO}_4(\text{g})$, which enhance the initial nucleation burst by an order of magnitude. Both of these cases (as well as case 18 discussed in section 4.2.4) gave initial nucleation rates exceeding $11,000 \text{ cm}^{-3} \text{ s}^{-1}$. In case 12, coagulation reduced particle number from $4,000,000 \text{ cm}^{-3}$ at $t = 0.1$ hour to $208,000 \text{ cm}^{-3}$ at $t = 1.0$ hour, further reducing it to $37,800 \text{ cm}^{-3}$ by $t = 8.0$ hours. Despite this very rapid coagulation the 6M–discrete model moment differences are similar to those found in case 3 and under a few percent. As a point of reference, it has been recently reported that peak aerosol concentrations can exceed $1,000,000 \text{ cm}^{-3}$ during nucleation bursts in coastal environments, which can last from 2 to 8 hours [O’Dowd, 2000]. It is unknown whether transient number concentrations at great as $4 \times 10^6 \text{ cm}^{-3}$ arise in the atmosphere, but this case (and others) shows that such conditions could be modeled accurately by 6M if encountered.

In case 12 the two models closely agree for N_c , mostly because of the fact that the lower limit of 0.005 set on the activated fraction was imposed in this case. At $t = 0$ hours, N_c is 192 cm^{-3} (6M) and 217 cm^{-3} (discrete model), with time-averaged values of 185 cm^{-3} (6M) and 189 cm^{-3} (discrete model).

4.2.4. Case 18. The initial conditions in case 18 are the same as those in case 15, except for the absence of preexisting aerosol, which has little impact on the results until the cloud encounter. However, during the cloud lifetime the small differences in the $t = 8.0$ hour moments in case 18 (compared to those in case 15) led to slightly different moment evolution, but different enough that MIDAS was able to perform size-

resolved activation more frequently in case 18 (size resolution in 85% of the time steps, rather than 40% in case 15). This increased frequency in size-resolved activation resulted in smaller 6M–discrete model differences in N_c and the moments in this case. The time-averaged N_c for the two models is 1638 cm^{-3} (6M) and 2031 cm^{-3} (discrete model) in case 18, compared to 1260 cm^{-3} (6M) and 2032 cm^{-3} (discrete model) in case 15. This case (and others) illustrates the importance of treating cloud activation in a size-resolved way.

4.3. Comparisons of Cloud Drop Number From 6M and the Discrete Model

We have discussed in section 4.2 cloud drop number in selected cases to better understand the moment evolution. Although prediction of N_c is not a primary objective in a CTM, it is still of interest to compare the average N_c obtained from 6M with values obtained from the discrete model for all test cases. N_c varies at each time step in a CTM, and Figure 5 shows N_c as averaged over the 2 hours (20 time steps) that clouds were specified to exist in the simulations. Over the 30 cases the time-averaged N_c ranges from ~ 30 to $3000 \text{ drops cm}^{-3}$, a physically reasonable result. The 6M tracks this variation in average N_c over the test cases with an average difference from the discrete model of -13% , an average magnitude of difference of 16% , and a maximum difference of -51% (case 9). For cases 3 and 9 we have discrete results with 500, 1000, and 2000 grid points, giving differences in average N_c of -8.8 , -7.2 , and -4.9% , respectively, for case 3, and -51.3 , -47.4 , and -44.9% , respectively, for case 9, showing modest reduction in the 6M–discrete model differences with increasing discrete resolution. These results for cases 3 and 9 are also summarized in Table 2.

4.4. MIDAS Surrogates for the Underlying Size Distributions

Figure 6 shows multimodal lognormal MIDAS surrogates obtained from the 6M moments corresponding to the initial and final distributions. As the tracking of moments inherently constrains numerical diffusion in size space and any excessive particle growth during condensation, the locations (in r space) of the surrogates agree well with the discrete distributions. In several cases only a single set of three lognormal modes could be retrieved, with the result that the surrogates are considerably sharper than the discrete PDFs. However, these are cases in which the underlying PDF is itself quite narrow and, as mentioned above, in a Eulerian model such narrow distributions will tend to be broadened because of mixing of aerosol samples that have evolved under different environmental conditions.

We note that the surrogates sometimes capture the bimodality of the PDF (e.g., case 3) but sometimes miss it (e.g., case 6). To our knowledge, there is no reason to expect the surrogates to capture the modality of the underlying PDF, as this information is not contained in the moments (see McGraw *et al.* [1998] for examples of identical moment sets with very different multimodality in the underlying PDFs). Nevertheless, in several cases (cases 14, 15, 17, 18, 20, 21, 23, and 24) the surrogates actually capture the shoulders on the PDFs, although in a few cases (cases 9, 26, and 29), shoulders appear in the surrogates that are absent in the PDFs. In any event, for calculation of integral aerosol properties, which are generally the desired objectives of such calculations, such fine structure in the PDF is of very little importance [McGraw *et al.*, 1998].

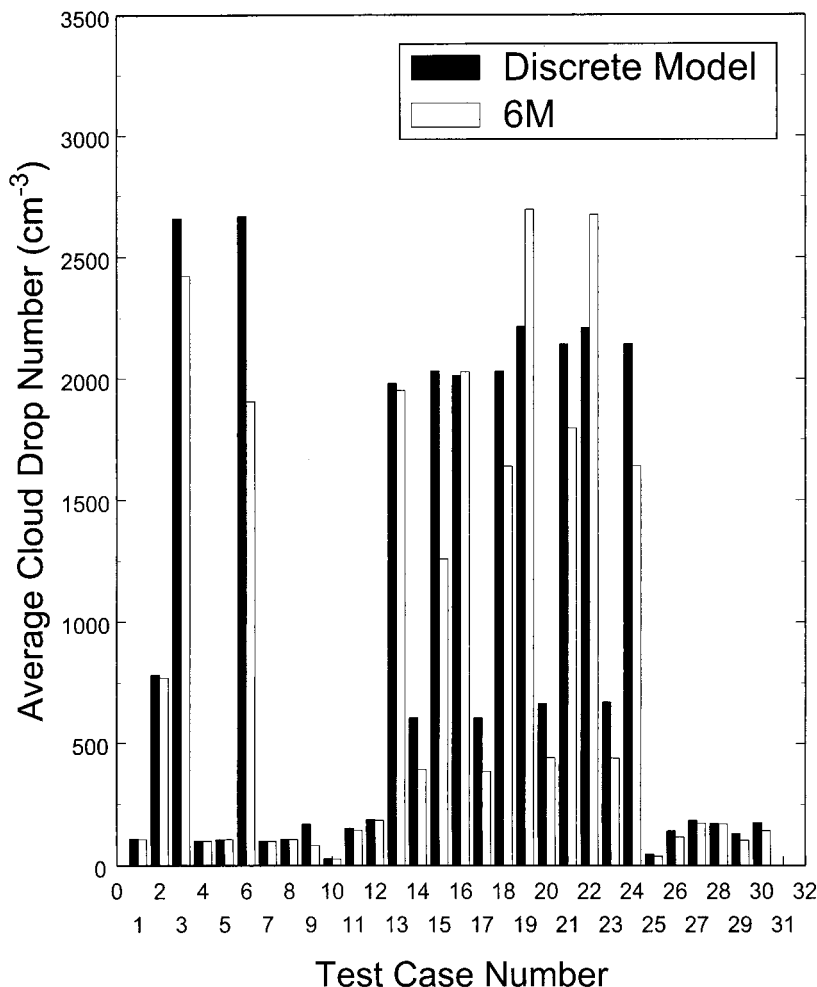


Figure 5. Average cloud drop number (drops cm^{-3}) for each test case from the discrete model and from 6M.

Considering the full set of test cases, MIDAS (or other) surrogates derived from moments can be expected to yield aerosol properties in good agreement with those of the underlying PDFs, especially bearing in mind the atypical narrowness of most of the final PDFs shown here, and the previously established accuracy of the MIDAS [Wright, 2000] and RMST [Yue *et al.*, 1997] approaches to computing aerosol optics from moments.

5. Model Performance, Implementation, and Summary

5.1. Model Performance and Further Development

The accuracy of the moments and aerosol properties obtained with 6M should be assessed in light of the uncertainties associated with the representation of other processes in CTMs: uncertainties in emissions, in deposition velocities, in precipitation rates, and in the algorithms for advection and other processes that mix aerosol samples from different cells. Uncertainties in the nucleation processes and rates are major limiting factors in modeling particle number and thus the modeling of mean particle properties, which require at least knowledge of aerosol number and one other moment (typically mass) for their determination. In light of these and other

uncertainties currently limiting the accuracy of CTMs the performance of 6M can be favorably viewed; 6M can be expected to represent known aerosol microphysics with an accuracy comparable to that obtained for other modeled processes.

Looking to improve the performance of 6M, the results of this study suggest that insuring a size-resolved cloud activation at all times is important. This can readily be accomplished with more elaborate decision structures in the activation algorithms.

Another area of improvement that will be undertaken in future model development will be to allow for the incorporation of additional species such as ammonia and organics, along with sulfuric acid and water, in the nucleation processes. Ternary nucleation models based on the revised classical nucleation theory are now emerging [Korhonen *et al.*, 1999] and need to be parameterized for use in atmospheric models.

5.2. Implementation Aspects

An important consideration in handling moment sets is the fact that the moments in a set are not independent quantities. Specifically, values of certain moments place constraints on the possible values of other moments (e.g., (normalized) μ_2 puts constraints on the possible values of (normalized) μ_1 , through $\mu_2 \geq (\mu_1)^2$; for a generalization of this result to a convexity condition on higher moments, see Feller [1971]). In practice,

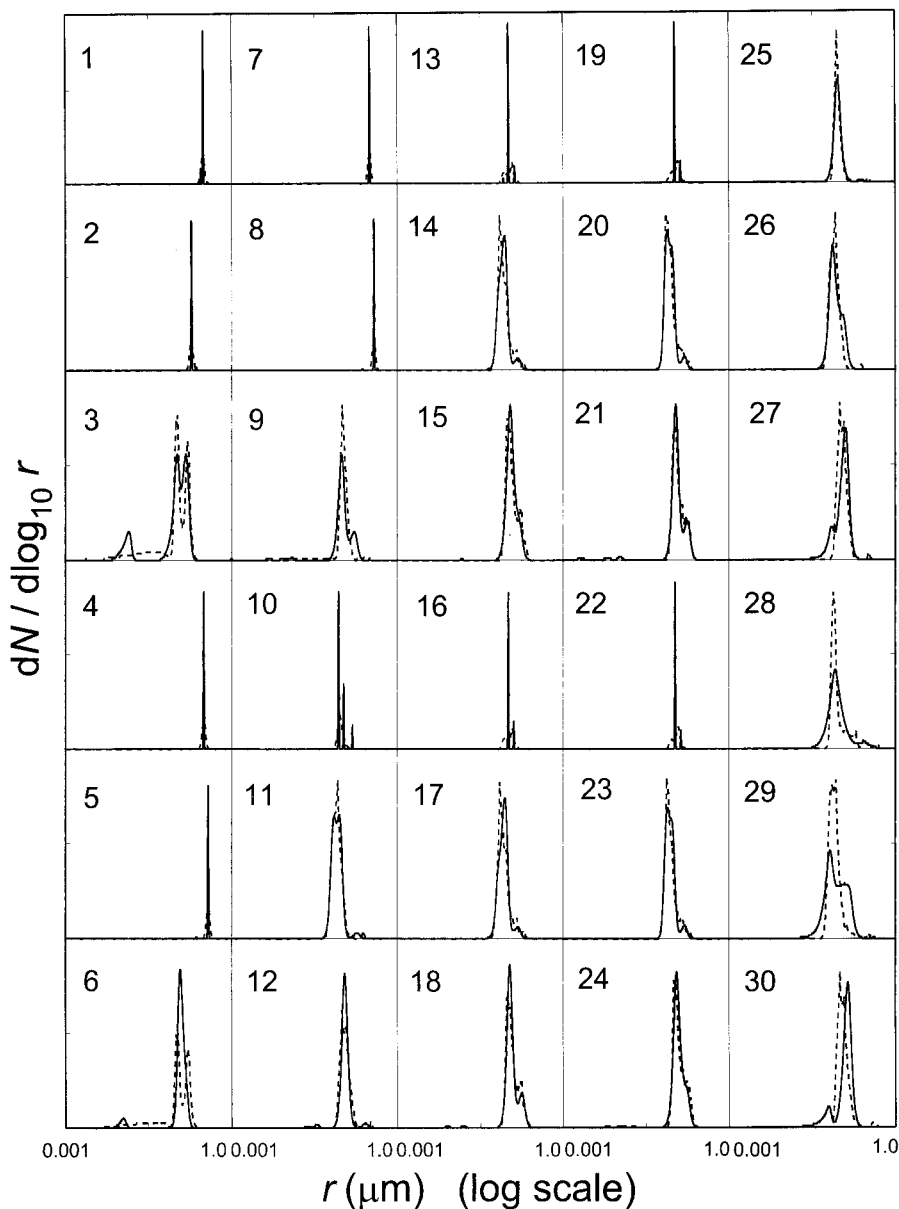


Figure 6. Final normalized distributions (at ambient RH) for each test case from the discrete model (dashed lines) and multimodal lognormal MIDAS surrogates derived from the final moments of 6M (solid lines). All distributions are plotted as equal-area plots, $dN/d \log_{10} r$ versus $\log_{10} r$. In each panel the distributions have been scaled to allow the plots to fill the panel vertically.

this impacts how aerosol samples (moment sets) are combined under advection and other processes in Eulerian models involving multiple grid cells. The approximations inherent in many 3-D advection algorithms can cause a valid set of moments (all constraints satisfied) to become invalid. Our approach to maintaining valid moments sets in CTMs has been to consider a moment set as a vector. Higher normalized moments are analogous to unit vectors, and aerosol number concentration provides the overall normalization. For aerosol evolution under advection, turbulent mixing, etc., information derived from the treatment of aerosol number can be used to update the higher normalized moments in a manner consistent with the evolution of particle number, by forming appropriate linear combinations of the higher moments in the cells involved. For example, for advection in the x direction (here

assuming operator splitting for the three directions) the updated value of μ_k ($k = 1-5$) in cell i is typically a linear combination of the values in cells $i - 1$, i , and $i + 1$. Thus one executes the advection routine for particle number only, while retaining the information needed for the coefficients of the required linear combinations. Although additional code must be added to the advection algorithm, significant execution time is saved. This approach has been implemented in conjunction with two versions of the Bott algorithm [Easter, 1993; Bott, 1989], and with these algorithms it is simple to form the requisite linear combinations [Wright et al., 2000].

We note that the routine for obtaining the quadrature abscissas and weights (ORTHOG) will sometimes fail when the underlying distribution is very narrow. In this case we chose to replace the input moments by the moments of a lognormal

distribution having the same particle number, mean radius, and mean volume as the input moments, and if these moments yield a lognormal standard deviation less than 1.001, σ_g is increased to 1.001, usually resulting in only small changes to the input moments.

Lastly, we note that ORTHOG will also fail if passed an invalid moment set, and we have in practice defined an invalid moment set as one that fails in ORTHOG. It is not difficult to imagine that evolving a set of delicately interrelated quantities in a CTM/GCM environment might be fraught with difficulties in preserving proper moment interrelationships. In our initial efforts at implementation of this approach in a CTM we were often dismayed by the ease with which a moment set could become invalid, but by the time implementation was complete we recognized that these moment constraints were actually an aide to the debugging process. Many possible coding or algorithmic errors will be caught by ORTHOG. In the subhemispheric simulations reported by Wright *et al.* [2000] there were 14 failures in ORTHOG in 6×10^7 calls of the subroutine during the first two modeled days (during the “spin-up” period) and no failures in the 10^9 calls during the remaining 28 days, a satisfying result illustrating that such “delicate” moment sets can be successfully propagated in CTMs.

5.3. Summary

We have described and evaluated an aerosol microphysical module, 6M, suitable for use in CTMs. A prototype of 6M was successfully implemented in a subhemispheric CTM [Wright *et al.*, 2000], and implementation of the module as described in this work is currently underway in regional and global CTMs. Although sufficient computing power may eventually be available to accurately represent the aerosol size distribution itself in CTMs and GCMs, we feel that for an indefinite period of time, accurate representations of aerosol evolution and properties based on moments will be useful in such large-scale models. This is especially likely considering that the next stage of model development will need to treat mixed aerosols, for which multivariate distribution functions tax PDF approaches excessively while, at least for the bivariate case, moments give a feasible parameterization. Given the huge demand on computing resources made by large-scale atmospheric models, accurate and compact representations of aerosol evolution and properties based on the MOM are finding increased application, with the treatment of aerosols limited more by knowledge of the underlying processes than by computing resources. This will especially be so when external mixtures of several aerosol populations require independent representation.

Acknowledgments. Work done at Duke was supported by grant NA76GP0350 from NOAA Office of Global Programs, and subcontract G-35-W62-G2 from Georgia Institute of Technology (principal grant R 826372-01-0 from EPA). Work done at BNL was supported in part by NASA through interagency agreement W-18,429 as part of its interdisciplinary program on tropospheric aerosols and in part by the Environmental Sciences Division of the U.S. Department of Energy (DOE) as part of the Atmospheric Chemistry Program and was performed under the auspices of DOE under contract DE-AC02-98CH10886.

References

Abdul-Razzak, H., S. J. Ghan, and C. Rivera-Carpio, A parameterization of aerosol activation, 1, Single aerosol type, *J. Geophys. Res.*, **103**, 6123–6131, 1998.

Barrett, J. C., and N. A. Webb, A comparison of some approximate

methods for solving the aerosol general dynamic equation, *J. Aerosol Sci.*, **29**, 31–39, 1998.

Bott, A., A positive definite advection scheme obtained by nonlinear renormalization of the advective fluxes, *Mon. Weather Rev.*, **117**, 1006–1015, 1989.

Easter, R. C., Two modified version of Bott’s positive definite numerical advection scheme, *Mon. Weather Rev.*, **121**, 297–304, 1993.

Feller, W., *An Introduction to Probability Theory and Its Applications*, vol. 2, p. 155, Wiley, New York, 1971.

Fitzgerald, J. W., W. A. Hoppel, and F. Gelbard, A one-dimensional sectional model to simulate multicomponent aerosol dynamics in the marine boundary layer, 1, Model description, *J. Geophys. Res.*, **103**, 16,085–16,102, 1998.

Friedlander, S. K., Dynamics of aerosol formation by chemical reaction, *Ann. N. Y. Acad. Sci.*, **404**, 354–364, 1983.

Fuchs, N. A., *The Mechanics of Aerosols*, translated by R. E. Daisley and M. Fuchs, Pergamon, New York, 1964.

Ghan, S. J., L. R. Leung, R. C. Easter, and H. Abdul-Razzak, Prediction of cloud droplet number in a general circulation model, *J. Geophys. Res.*, **102**, 21,777–21,794, 1997.

Giorgi, F., A particle dry-deposition parameterization scheme for use in tracer transport models, *J. Geophys. Res.*, **91**, 9794–9806, 1986.

Hegg, D. A., D. S. Covert, and C. F. Kapustin, Modeling a case of particle nucleation in the marine boundary layer, *J. Geophys. Res.*, **97**, 9851–9857, 1992.

Heintzenberg, J., H. Muller, J. Quenzel, and E. Thomalla, Information contents of optical data with respect to aerosol properties: Numerical studies with a randomized minimization-search-technique inversion algorithm, *Appl. Opt.*, **20**, 1308–1315, 1981.

Hoppel, W. A., G. M. Frick, J. W. Fitzgerald, and R. E. Larson, Marine boundary layer measurements of new particle formation and the effects nonprecipitating clouds have on aerosol size distribution, *J. Geophys. Res.*, **99**, 14,443–14,459, 1994.

Hulburt, H. M., and S. Katz, Some problems in particle technology: A statistical mechanical formulation, *Chem. Eng. Sci.*, **19**, 555–574, 1964.

Jacobsen, M. Z., R. P. Turco, E. J. Jensen, and O. B. Toon, Modeling coagulation among particles of different composition and size, *Atmos. Env.*, **28**, 1327–1338, 1994.

Jaeger-Voirol, A., and P. Mirabel, Heteromolecular nucleation in the sulfuric acid-water system, *Atmos. Environ.*, **23**, 2053–2057, 1989.

Korhonen, P., M. Kulmala, A. Laaksonen, Y. Viisanen, R. McGraw, and J. H. Seinfeld, Ternary nucleation of H₂SO₄, NH₃, and H₂O in the atmosphere, *J. Geophys. Res.*, **104**, 26,349–26,353, 1999.

Kreidenweis, S. M., J. E. Penner, F. Yin, and J. H. Seinfeld, The effects of dimethylsulfide upon marine aerosol concentrations, *Atmos. Environ.*, **Part A**, **25**, 2501–2511, 1991.

McGraw, R., Description of aerosol dynamics by the quadrature method of moments, *Aerosol Sci. Technol.*, **27**, 255–265, 1997.

McGraw, R., and J. H. Saunders, A condensation feedback mechanism for oscillatory nucleation and growth, *Aerosol Sci. Technol.*, **3**, 367–380a, 1984.

McGraw, R., P. I. Huang, and S. E. Schwartz, Optical properties of atmospheric aerosols from moments of the particle size distribution, *Geophys. Res. Lett.*, **22**, 2929–2932, 1995.

McGraw, R., S. Nemesure, and S. E. Schwartz, Properties and evolution of aerosols with size distributions having identical moments, *J. Aerosol Sci.*, **29**, 761–772, 1998.

O’Dowd, C. D., New particle formation and fate in the coastal environment (PARFORCE): Objectives and initial achievement, *Rep. Ser. in Aerosol Sci.* **48**, pp. 5–11, Finn. Assoc. for Aerosol Sci., Helsinki, 2000.

Pratsinis, S. E., Simultaneous nucleation, condensation, and coagulation in aerosol reactors, *J. Colloid Interface Sci.*, **124**, 416–427, 1988.

Press, W. H., S. A. Teukolsky, W. T. Vetterling, and B. P. Flannery, *Numerical Recipes in FORTRAN*, Cambridge Univ. Press, N.Y., 1992.

Raes, F., and R. Van Dingenen, Simulations of condensation and cloud condensation nuclei from biogenic SO₂ in the remote marine boundary layer, *J. Geophys. Res.*, **97**, 12,901–12,912, 1992.

Raes, F., A. Saltelli, and R. Van Dingenen, Modeling formation and growth of H₂SO₄-H₂O aerosols: Uncertainty analysis and experimental evaluation, *J. Aerosol Sci.*, **23**, 759–771, 1992.

Russell, L., and J. H. Seinfeld, Size- and composition-resolved externally mixed aerosol model, *Aerosol Sci. Technol.*, **28**, 403–416, 1998.

Slinn, W. G. N., Air-to-sea transfer of particles, in *Air-Sea Exchange of*

- Gases and Particles*, edited by P. S. Liss and W. G. N. Slinn, pp. 299–405, D. Reidel, Norwell, Mass., 1983.
- Tandon, P., and D. E. Rosner, Monte-Carlo simulation of particle aggregation and simultaneous restructuring, *J. Colloid Interface Sci.*, *213*, 273–286, 1999.
- Tang, I. N., and H. R. Munkelwitz, Water activities, densities, and refractive indices of aqueous sulfates and sodium nitrate droplets of atmospheric importance, *J. Geophys. Res.*, *99*, 18,801–18,808, 1994.
- Whitby, E., and P. H. McMurry, Modal aerosol dynamics modeling, *Aerosol Sci. Technol.*, *27*, 673–688, 1997.
- Whitby, K., The physical characteristics of sulfur aerosols, *Atmos. Environ.*, *12*, 125–159, 1978.
- Wright, D. L., Retrieval of optical properties of atmospheric aerosols from moments of the particle size distribution, *J. Aerosol Sci.*, *31*, 1–18, 2000.
- Wright, D. L., R. McGraw, C. M. Benkovitz, and S. E. Schwartz, Six-moment representation of multiple aerosol populations in a sub-hemispheric chemical transformation model, *Geophys. Res. Lett.*, *27*, 967–970, 2000.
- Wright, D. L., R. McGraw, and D. E. Rosner, Bivariate extension of the quadrature method of moments for modeling simultaneous coagulation and sintering of particle populations, *J. Colloid Interface Sci.*, in press, 2001.
- Yue, G. K., J. Lu, V. A. Mohnen, P.-H. Wang, V. K. Saxena, and J. Anderson, Retrieving aerosol optical properties from moments of the particle size distribution, *Geophys. Res. Lett.*, *24*, 651–654, 1997.
-
- P. S. Kasibhatla and D. L. Wright, Nicholas School of the Environment, Duke University, Box 90328, Durham, NC 27705. (psk@duke.edu)
- R. McGraw and S. E. Schwartz, Atmospheric Sciences Division, Department of Applied Science, Brookhaven National Laboratory, Upton, NY 11973. (rlm@aerosol.das.bnl.gov; ses@bnl.gov; dwright@bnl.gov)

(Received October 13, 2000; revised February 16, 2001; accepted February 22, 2001.)

